Electronic Supplementary Information

Does Fe^{2+} in olivine-based interstellar grains play any role in the formation of H_2? Atomistic insights from DFT periodic simulations

Javier Navarro-Ruiz,[a] Piero Ugliengo,[b] Mariona Sodupe,[a] and Albert Rimola[a]*

[a] *Departament de Química, Universitat Autònoma de Barcelona, 08193 Bellaterra, Spain*

[b] *Dipartimento di Chimica and NIS – Nanostructured Interfaces and Surfaces – Interdepartment Centre, Università degli Studi di Torino, Via P. Giuria 7, 10125, Torino, Italy*

E-mail corresponding author: albert.rimola@uab.cat

Extended Computational Details

All periodic calculations have been performed with the *ab initio* CRYSTAL09 code.[1,2] This code implements the Hartree−Fock and Kohn−Sham self-consistent field method based on localized Gaussian Type Orbitals (GTO) for periodic systems.[3] The self-consistent field (SCF) calculations and geometry optimizations were performed with the B3LYP-D2* functional, which includes an empirical *a posteriori* correction term proposed by Grimme[4] to account for dispersion forces (missed in the pure B3LYP[5,6] method), but whose initial parametrization (D2) was modified for extended systems (D2*),[7] to provide accurate results for the calculations of cohesive energies of molecular crystals and of adsorption processes within a periodic treatment;[8–10] and also with the BHLYP[11] functional, because it better describes the electronic structure of Fe-containing systems, as it is shown with the calibration study (see Table S1). Transition state (TS) search has been performed using the distinguished reaction coordinate (DRC) technique as implemented in CRYSTAL09, which has been proven to be robust and efficient enough for the proton jump of non-hydrated and hydrated acidic zeolites.[12] The activated complex structures corresponding to the TS have been checked by ensuring that only one imaginary frequency resulted by the Hessian matrix diagonalization. All calculations involving one H atom have been run as open-shell systems based on the unrestricted formalism, whereas for dihydrogen adsorption the starting guess was open shell broken symmetry but collapsed to the closed shell system. Geometry optimizations have been performed in the *P1* group symmetry (no symmetry), in order to ensure the maximum degrees of freedom during the optimization. Net charges and electron spin densities on the atoms were derived from the Mulliken population analysis.

The multi-electron wave function is described by linear combination of crystalline orbitals, which in turn are expanded in terms of GTO basis sets. Two different Gaussian basis sets have been adopted: (i) a B1 basis set described by the following all-electron contractions: (8s)–(831sp)–(1d) for Si; (6s)–(31sp)–(1d) for O; (6s)–(631sp)–(1d) for the top-layer Mg atoms (standard 6-31G(d,p) Pople basis set); (8s)–(61sp)–(1d) for the remaining Mg atoms; and (6s)–(6631sp)–(31d)–(1f) for Fe; and (ii) a B2 basis set described by the larger all-electron contractions: (8s)–(6311sp)–(1d) for Si; (8s)–(411sp)–(1d) for O; (631111s)–(42111p)–(1d) for the top-layer Mg atoms (standard 6-311G(d,p) Pople basis set); (8s)–(511sp)–(1d) for the remaining Mg atoms; and (62111111s)–(331111p)–(311d) for Fe; these basis functions were already used in

previous works focused on the forsterite[13–15] and fayalite[16] bulk properties. For all calculations, a TZP basis set from Ahlrichs and coworkers[17] has been used for the H atoms. All the geometry optimizations have been carried out using the B1 basis sets and the energy is refined with single-point energy calculations at B2 onto the optimized B1 geometries (hereafter referred as B2//B1). In a previous work,[18] we showed that B2//B1 energy values are almost indistinguishable from those at B2//B2 level.

We set the shrinking factor of the reciprocal space net, defining the mesh of *k* points in the irreducible Brillouin zone,[19] to 5 and 20 for B1 and B2 calculations, respectively, requiring the diagonalization of the Hamiltonian matrix in 3 and 6 *k* points, respectively. The accuracy of both Coulomb and exchange series was set to values of overlap integrals of 10^{-6} and 10^{-16} for both B1 and B2. A pruned (75, 974) grid has been used for the Gauss–Legendre and Lebedev quadrature schemes in the evaluation of functionals.[2,20] The condition to achieve SCF convergence between two subsequent cycles was set to 10^{-7} Hartree. Relaxations of both the internal atomic coordinates and the unit cell parameters for the bare surface, on the one hand, and relaxations of only the internal atomic coordinates keeping the lattice parameters fixed at the bare surface for the rest of the calculations, on the other hand, were carried out within the same run by means of analytical energy gradients[21] using a quasi-Newton algorithm, in which the quadratic step (Broyden−Fletcher−Goldfarb−Shanno Hessian updating scheme, BFGS)[22–25] is combined with a linear one as proposed by Schlegel.[26]

H atom adsorption and recombination was only considered on the top surface of the slabs, since this greatly simplifies the localization of TS structures. We are conscious that this approach breaks the symmetry of the system with, nevertheless, a negligible effect on the energy profiles. The adsorption energies (ΔE) per mole of an H atom and per unit cell were computed as:

$$\Delta E = E_{SH} - (E_S + E_H) \quad (1)$$

where E_{SH} is the energy of the relaxed unitary cell containing the forsterite surface S in interaction with the H atom, E_S is the energy of the relaxed unitary cell of the free forsterite surface, and E_H is the energy of the free H atom.

CRYSTAL09 computes the zero-point energy (ZPE) corrections and thermodynamic quantities using the standard statistical thermodynamics formulae based on partition functions derived from the harmonic oscillator approximations, which are used to correct the adsorption energy values by temperature effects. The corresponding vibrational frequencies are calculated by obtaining the eigenvalues from diagonalization of the mass-weighted Hessian matrix at Γ point (point $k = 0$ in the first Brillouin zone, called the central zone). The mass-weighted Hessian matrix was obtained by numerical differentiation (central-difference formula) of the analytical first energy derivatives, calculated at geometries obtained by displacing, in turn, each of the $3N$ equilibrium nuclear coordinates by a small amount, $u = 0.003$ Å (N is the number of atoms).[27] For the considered systems in this work, building up the full mass-weighted Hessian matrix would have been very expensive, so that only a portion of the dynamical matrix was computed by considering the displacements of a subset of atoms; *i.e.*, the H atoms and the first and second-layer atoms of the surface.

Quantum tunnelling, a purely quantum mechanical effect, can play a significant role in the studied processes allowing chemical reactions to occur at significant rates at low temperatures, which classically would have negligible rates,[28] and the fact that they involve H atoms. The probability for a given system to tunnel through a reaction barrier depends primarily on the curvature of the barrier, which is controlled by the transition vibrational frequency and, to a lower degree, on the height of the barrier. The importance of tunnelling for a specific reaction can be estimated by employing the tunnelling crossover temperature T_X, which can be calculated using the formula by Fermann and Auerbach:[29]

$$T_X = \frac{h\nu^{\ddagger} i \Delta U_0^{\ddagger} / k_B}{2\pi \Delta U_0^{\ddagger} - h\nu^{\ddagger} i \ln 2} \qquad (2)$$

with $\nu^{\ddagger}$ the absolute value of the imaginary frequency of the transition mode, h the Plank's constant, $\Delta U_0^{\ddagger}$ the zero-point energy-corrected barrier and k_B the Boltzmann's constant. T_X generally marks the temperature below which tunnelling becomes dominant and above which tunnelling becomes negligible. Moreover, rate constants in a semi-classical way (k^{SC-TST}) are calculated, in which tunnelling contributions are accounted for by introducing the transmission coefficient ($\Gamma(T)$) developed by Fermann

and Auerbach[29] into the classical Eyring rate constant (k^{TST}) from the standard TST using partition functions:

$$k^{SC-TST} = \Gamma(T) \times k^{TST} \tag{3}$$

$$k^{TST} = \left(\frac{k_B T}{h}\right) e^{-\frac{\Delta G^{\ddagger}}{k_B T}} \tag{4}$$

$$\Gamma(T) = e^{\Delta {U_0}^{\ddagger}/k_B T} e^{-2\pi \Delta {U_0}^{\ddagger}/h\nu^{\ddagger} i} \left(1 + \frac{2\pi k_B T}{h\nu^{\ddagger} i}\right) \tag{5}$$

where $\Delta G^{\ddagger}$ is the free-energy barrier calculated at the temperature T.

References

1 R. Dovesi, R. Orlando, B. Civalleri, C. Roetti, V. R. Saunders and C. M. Zicovich-Wilson, *Zeitschrift für Krist.*, 2004, **220**, 571–573.
2 R. Dovesi, V. R. Saunders, C. Roetti, R. Orlando, C. M. Zicovich-Wilson, F. Pascale, B. Civalleri, K. Doll, N. M. Harrison, I. J. Bush, P. D'Arco and M. Llunell, *CRYSTAL09 User's Manual*, University of Torino, Torino, 2010.
3 C. Pisani, R. Dovesi and C. Roetti, *Hartree-Fock Ab Initio Treatment of Crystalline Systems*, Springer-Verlag, Berlin, 1988.
4 S. Grimme, *J. Comput. Chem.*, 2006, **27**, 1787–1799.
5 A. D. Becke, *J. Chem. Phys.*, 1993, **98**, 5648–5652.
6 C. Lee, W. Yang and R. G. Parr, *Phys. Rev. B*, 1988, **37**, 785–789.
7 B. Civalleri, C. M. Zicovich-Wilson, L. Valenzano and P. Ugliengo, *CrystEngComm*, 2008, **10**, 405–410.
8 A. D. Boese and J. Sauer, *Phys. Chem. Chem. Phys.*, 2013, **15**, 16481–16493.
9 P. Ugliengo and A. Damin, *Chem. Phys. Lett.*, 2002, **366**, 683–690.
10 B. Civalleri, L. Maschio, P. Ugliengo and C. M. Zicovich-Wilson, *Phys. Chem. Chem. Phys.*, 2010, **12**, 6382–6386.
11 A. D. Becke, *J. Chem. Phys.*, 1993, **98**, 1372–1377.
12 A. Rimola, C. M. Zicovich-Wilson, R. Dovesi and P. Ugliengo, *J. Chem. Theory Comput.*, 2010, **6**, 1341–1350.
13 Y. Noël, M. Catti, P. D'Arco and R. Dovesi, *Phys. Chem. Miner.*, 2006, **33**, 383–393.
14 M. de La Pierre, R. Orlando, L. Maschio, K. Doll, P. Ugliengo and R. Dovesi, *J. Comput. Chem.*, 2011, **32**, 1775–1784.
15 M. de La Pierre, C. Carteret, R. Orlando and R. Dovesi, *J. Comput. Chem.*, 2013, **34**, 1476–1485.
16 Y. Noël, M. de La Pierre, L. Maschio, M. Rérat, C. M. Zicovich-Wilson and R. Dovesi, *Int. J. Quantum Chem.*, 2012, **112**, 2098–2108.
17 A. Schäfer, H. Horn and R. Ahlrichs, *J. Chem. Phys.*, 1992, **97**, 2571–2577.
18 J. Navarro-Ruiz, M. Sodupe, P. Ugliengo and A. Rimola, *Phys. Chem. Chem. Phys.*, 2014, **16**, 17447–17457.
19 H. J. Monkhorst and J. D. Pack, *Phys. Rev. B*, 1976, **13**, 5188–5192.

20 F. Pascale, S. Tosoni, C. M. Zicovich-Wilson, P. Ugliengo, R. Orlando and R. Dovesi, *Chem. Phys. Lett.*, 2004, **396**, 308–315.
21 K. Doll, *Comput. Phys. Commun.*, 2001, **137**, 74–88.
22 C. G. Broyden, *J. Inst. Math. its Appl.*, 1970, **6**, 76–90.
23 R. Fletcher, *Comput. J.*, 1970, **13**, 317–322.
24 D. Goldfarb, *Math. Comput.*, 1970, **24**, 23–26.
25 D. F. Shanno, *Math. Comput.*, 1970, **24**, 647–656.
26 B. Civalleri, P. D'Arco, R. Orlando, V. R. Saunders and R. Dovesi, *Chem. Phys. Lett.*, 2001, **348**, 131–138.
27 F. Pascale, C. M. Zicovich-Wilson, F. López Gejo, B. Civalleri, R. Orlando and R. Dovesi, *J. Comput. Chem.*, 2004, **25**, 888–897.
28 V. I. Goldanskii, *Nature*, 1979, **279**, 109–115.
29 J. T. Fermann and S. Auerbach, *J. Chem. Phys.*, 2000, **112**, 6787–6794.

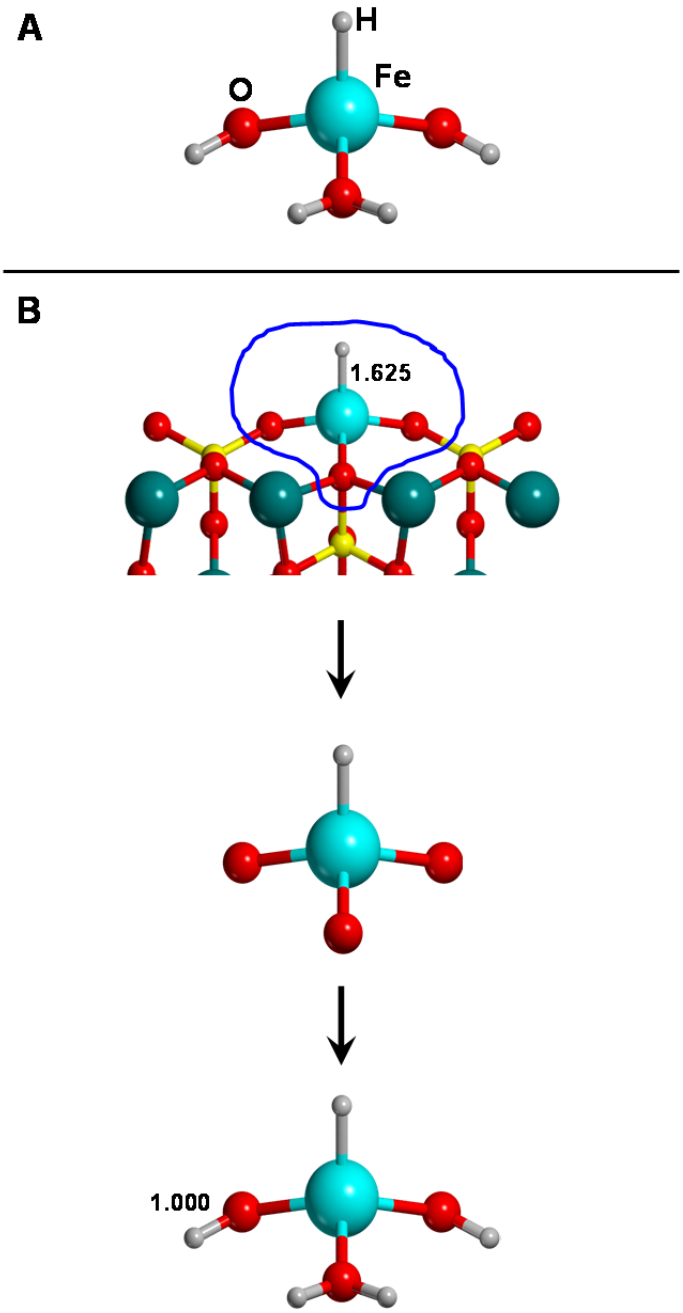

Figure S1. (A) Cluster model adopted for the calibration study, in which one H atom is adsorbed on the Fe ion. (B) The cluster derives from the first coordination sphere around the Fe ion of the 010-Fe1 complex (inset structure of the first image) optimized at BHLYP level. The dangling bonds were saturated by H atoms at distances of 1.000 Å with the corresponding O atoms. The formula of the cluster is $[Fe(OH)_2(H_2O)]$, in which two OH^- groups are present to ensure the electroneutrality of the cluster as in the periodic surface.

Table S1. Energy differences between the sextet and quartet electronic states (E_{sextet} - $E_{quartet}$) obtained at different DFT methods and at CCSD(T) (in kJ mol^{-1}). Basis set employed in the DFT methods: 6-31G(d,p) Pople basis set for H and O, and a Wachters basis set with f functions for polarization for Fe. Basis set employed at CCSD(T): aug-cc-pVTZ for H and O atoms, and Roos Augmented Triple Zeta ANO for Fe. Calculations are based on single-point energy calculations onto the cluster model at the geometry of the 010-Fe1 complex optimized with the BHLYP method.

Method	% of Exact Exchange	$E_{sextet} - E_{quartet}$
BLYP	0	-0.4
G96LYP	0	-2.3
BP86	0	-2.7
BPW91	0	-7.7
PBE	0	-9.4
TPSSh	10	-27.9
B3LYP	20	-37.4
B3PW91	20	-44.2
B97H	21	-43.9
B1LYP	25	-46.8
HSE06	25	-52.4
mPW1PW91	25	-53.0
PBE0	25	-55.5
mPWB1K	44	-78.5
BHLYP	50	-88.5
KMLYP	55	-99.5
CCSD(T)	---	-71.3

Table S2. Second ionization energies (in kcal mol^{-1}) for Mg and Fe calculated at B3LYP, BHLYP, and CCSD(T) by employing Roos Augmented Triple Zeta ANO as a basis set. Experimental values from NIST are also included.

Method	$Mg^{+} \rightarrow Mg^{2+}$	$Fe^{+} \rightarrow Fe^{2+}$
B3LYP	357.2	380.3
BHLYP	352.9	368.7
CCSD(T)	341.9	368.6
Experimental	346.7	373.6

Table S3. Adsorption energies (in kJ mol^{-1}) calculated at the B3LYP-D2*/B2//B3LYP-D2*/B1 and BHLYP-D2*/B2//BHLYP/B1 level, respectively, for the first H adsorption processes on Ol(010) to form the 010–Fe1, 010–O1, 010–O2 and 010–Mg1 adducts at sextet and quartet spin state. Pure potential adsorption energy (ΔE_{el}), contribution of dispersion to the adsorption energy (ΔE_{D2^*}), DFT-D2* adsorption energy ($\Delta E = \Delta E_{el} + \Delta E_{D2^*}$), contribution of zero-point energy to the adsorption energy (ΔZPE) and ZPE-corrected adsorption energy ($\Delta U_0 = \Delta E + \Delta ZPE$).

Adduct	Method	Spin	ΔE_{el}	ΔE_{D2^*}	ΔE	ΔZPE	ΔU_0
010–Fe1	B3LYP-D2*	Sextet	-185.7	-2.5	-188.2	16.3	-171.9
		Quartet	-131.0	-0.7	-131.7	17.3	-114.4
	BHLYP-D2*	Sextet	-161.8	-2.5	-164.3	18.1	-146.2
		Quartet	-60.9	-0.7	-61.6	18.7	-42.9
010–O1	B3LYP-D2*	Sextet	-53.0	-1.2	-54.2	27.3	-26.9
		Quartet	-54.5	-1.2	-55.7	27.8	-27.9
	BHLYP-D2*	Sextet	-67.9	-1.2	-69.1	28.8	-40.3
		Quartet	-38.7	-1.2	-39.9	28.7	-11.2
010–O2	B3LYP-D2*	Sextet	-67.2	-0.1	-67.3	26.4	-40.9
		Quartet	-67.2	-0.1	-67.3	26.2	-41.1
	BHLYP-D2*	Sextet	-57.8	-0.1	-57.9	27.3	-30.6
		Quartet	-57.8	-0.1	-57.9	28.0	-29.9
010–Mg1	B3LYP-D2*	Sextet	-6.5	-2.6	-9.1	3.7	-5.4
		Quartet	-6.5	-2.6	-9.1	3.7	-5.4
	BHLYP-D2*	Sextet	-4.7	-2.6	-7.3	3.8	-3.5
		Quartet	-4.8	-2.6	-7.4	3.6	-3.8

Table S4. Net charges and electronic spin densities on the H, Fe and Mg atoms, and the sum of the spin density values of the O atoms closest to H, computed at BHLYP-D2*/B2//BHLYP/B1 level for the different singly-H adsorptions on Ol(010) at sextet spin state.

	Charge				Spin			
	H	Fe	Mg	O	H	Fe	Mg	O
010–Fe1	-0.26	+1.35	+1.10	-1.18	0.19	4.58	0.00	0.23
010–O1	+0.32	+0.52	+1.11	-1.13	0.01	4.93	0.00	0.06
010–O2	+0.33	+1.20	+0.45	-1.13	0.01	3.93	0.95	0.11
010–Mg1	+0.06	+1.18	+1.02	-1.19	0.96	3.90	0.02	0.12

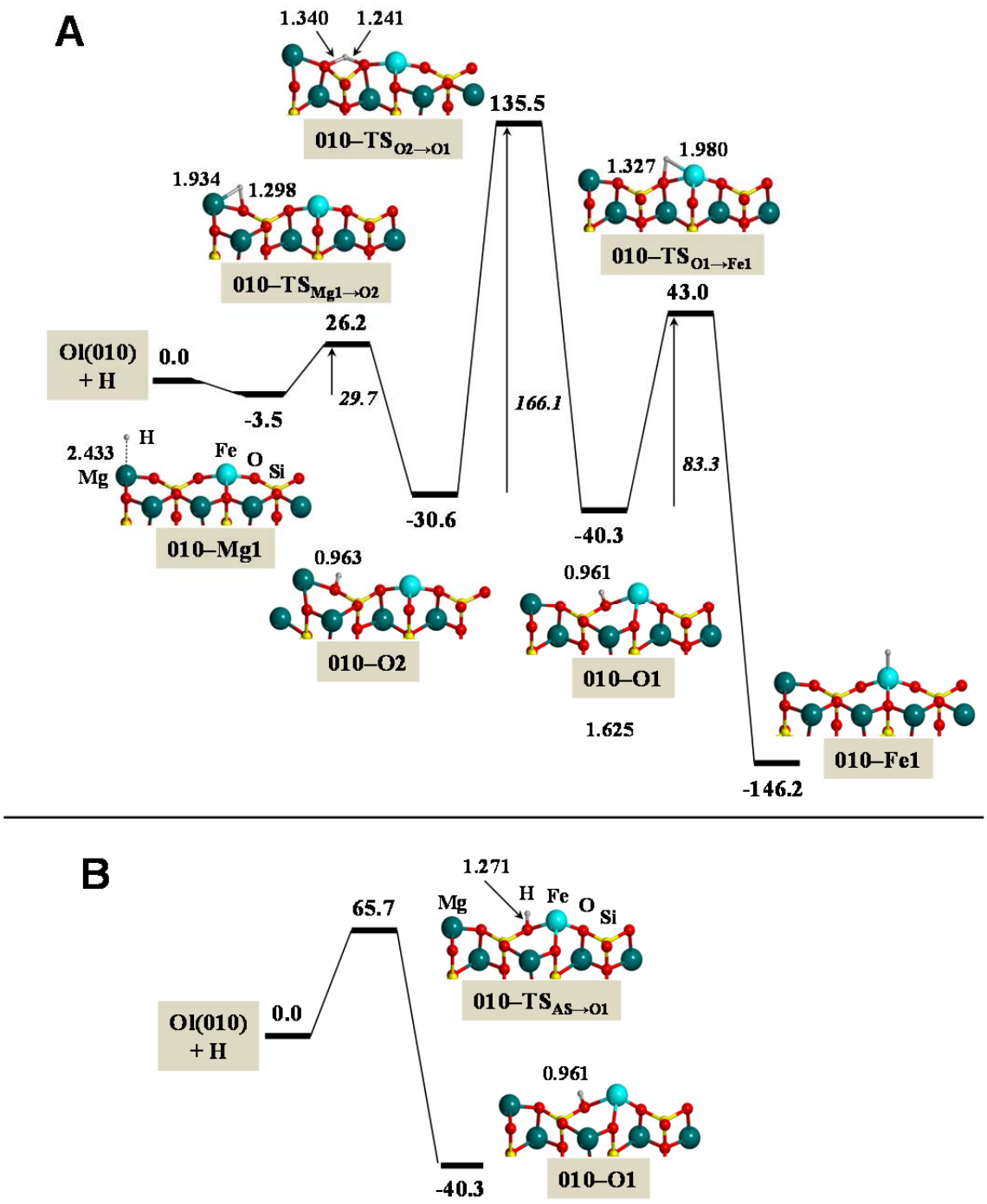

Figure S2. BHLYP-D2*//BHLYP-energy profiles including ZPE corrections (in kJ mol^{-1}) for the interconversion between the different adsorption states adopting the 010-Mg1 → 010-O2 → 010-O1 → 010-Fe1 sequence (A) and direct H adsorption to form 010-O1 (A). Relative energies are referenced with respect to Ol(010) + H zero-energy asymptote. Bond distances in Å.

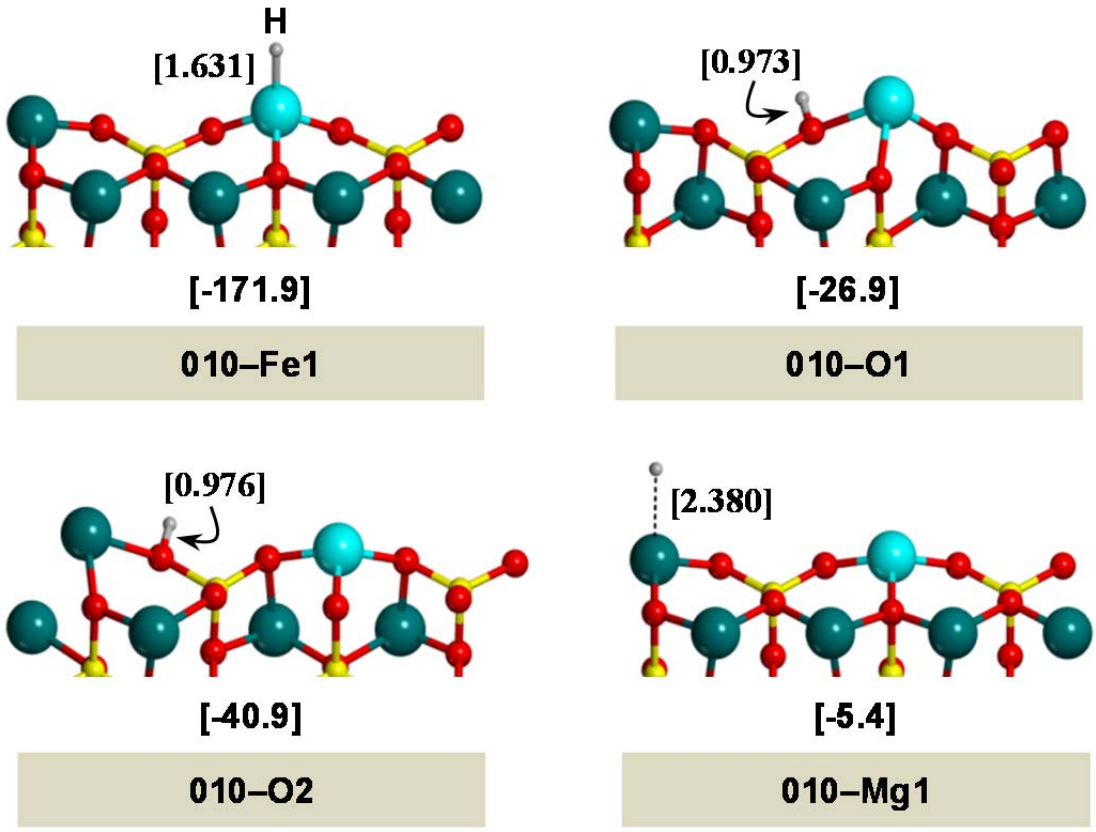

Figure S3. B3LYP-D2*-optimized geometries of the different complexes for the H adsorption on the Fe-containing surface at the sextet state. Bond distances (in Å) and adsorption energies including zero-point energy corrections (in kJ mol^{-1}) are also included.

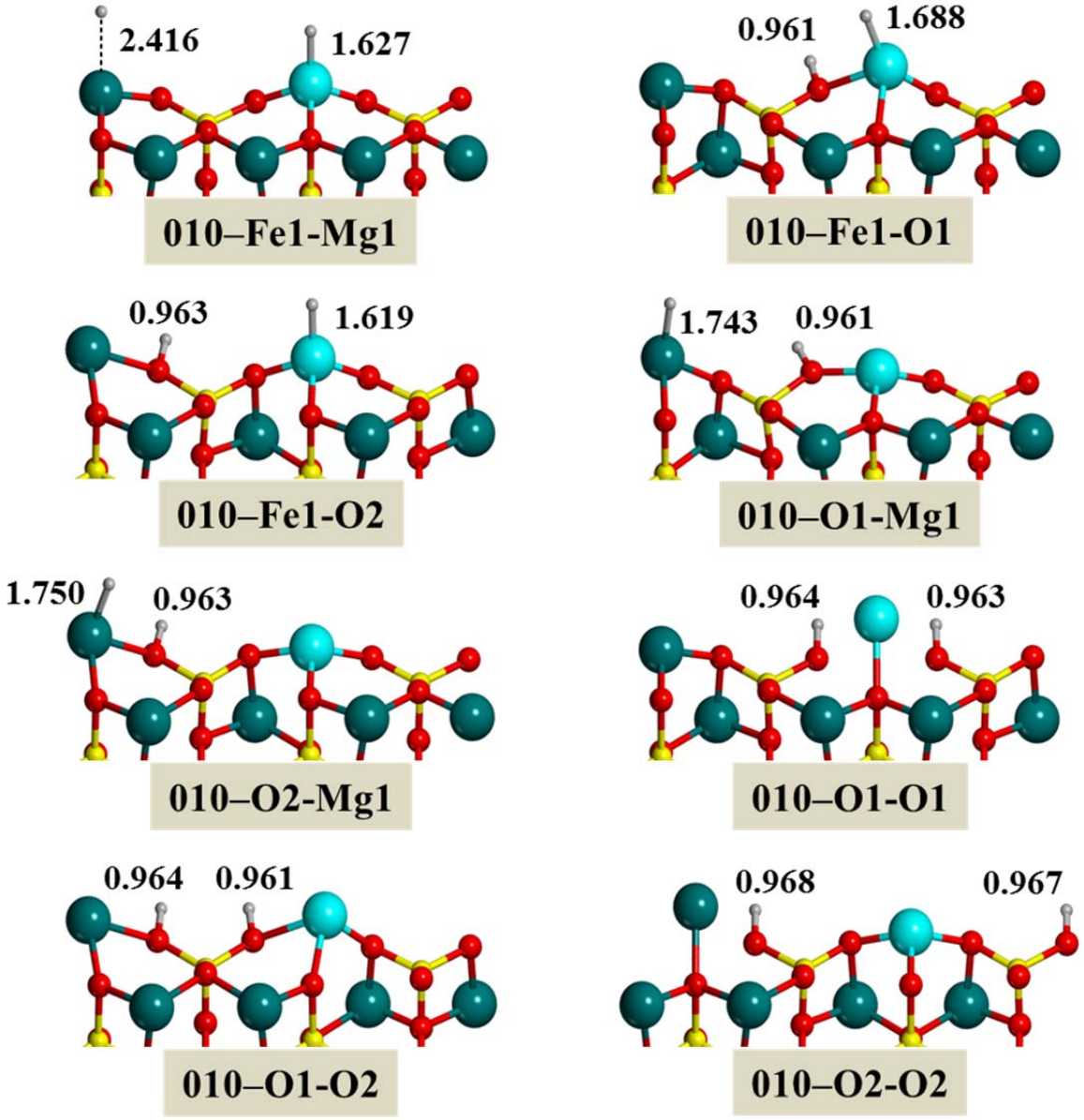

Figure S4. BHLYP-optimized geometries of the different complexes resulting from the adsorption of two H atoms on Ol(010) at quintet spin state (010–Fe1-Mg1, 010–Fe1-O1, 010–Fe1-O2, 010–O1-Mg1, 010–O2-Mg1, 010–O1-O1, 010–O1-O2 and 010–O2-O2). Bond distances in Å.

Table S5. Adsorption energies (in kJ mol^{-1}) calculated at the B3LYP-D2*/B2//B3LYP-D2*/B1 and BHLYP-D2*/B2//BHLYP/B1 level, respectively, for the global H adsorption processes on Ol(010) to form the 010–Fe1-Mg1, 010–Fe1-O1, 010–Fe1-O2, 010–O1-Mg1, 010–O2-Mg1, 010–O1-O1, 010–O1-O2 and 010–O2-O2 complexes at quintet spin state.

Reaction	Method	ΔE_{el}	ΔE_{D2^*}	ΔE	ΔZPE	ΔU_0
Ol(010) + 2H → 010–Fe1-Mg1	B3LYP-D2*	-192.8	-5.1	-197.9	20.2	-177.7
	BHLYP-D2*	-172.4	-5.1	-177.5	21.1	-156.4
Ol(010) + 2H → 010–Fe1-O1	B3LYP-D2*	-419.3	-4.7	-424.0	43.0	-381.0
	BHLYP-D2*	-421.5	-4.7	-426.2	44.8	-381.4
Ol(010) + 2H → 010–Fe1-O2	B3LYP-D2*	-337.7	-1.6	-339.3	42.4	-296.9
	BHLYP-D2*	-214.4	-1.6	-216.0	44.9	-171.1
Ol(010) + 2H → 010–O1-Mg1	B3LYP-D2*	-338.9	-2.0	-340.9	41.4	-299.5
	BHLYP-D2*	-325.5	-2.0	-327.5	42.3	-285.2
Ol(010) + 2H → 010–O2-Mg1	B3LYP-D2*	-408.6	-4.8	-413.4	41.3	-372.1
	BHLYP-D2*	-398.8	-4.8	-403.6	43.0	-360.6
Ol(010) + 2H → 010–O1-O1	B3LYP-D2*	-173.8	-12.5	-186.3	51.8	-134.5
	BHLYP-D2*	-160.3	-12.5	-172.8	55.0	-117.8
Ol(010) + 2H → 010–O1-O2	B3LYP-D2*	-87.6	-0.8	-88.4	52.0	-36.4
	BHLYP-D2*	-80.8	-0.8	-81.6	53.7	-27.9
Ol(010) + 2H → 010–O2-O2	B3LYP-D2*	-130.8	-9.6	-140.4	50.2	-90.2
	BHLYP-D2*	-108.6	-9.6	-118.2	53.1	-65.1

Table S6. Net charges and electronic spin densities on the H, Fe and Mg atoms, and the sum of the spin density values of the O atoms closest to H, computed at BHLYP-D2*/B2//BHLYP/B1 level for the different doubly-H adsorptions on Ol(010) at quintet spin state (H^{1st} and H^{2nd} denotes the first and second H position according to the nomenclature of the complex, respectively).

	Charge					Spin				
	H^{1st}	H^{2nd}	Fe	Mg	O	H^{1st}	H^{2nd}	Fe	Mg	O
010–Fe1-Mg1	-0.27	+0.07	+1.35	+1.02	-1.18	0.19	-0.96	4.59	-0.03	0.21
010–Fe1-O1	-0.43	+0.33	+0.97	+1.11	-1.13	-0.04	0.00	4.00	0.00	0.04
010–Fe1-O2	-0.23	+0.34	+1.34	+0.46	-1.12	0.20	-0.01	4.57	-0.96	0.19
010–O1-Mg1	+0.34	-0.31	+1.20	+0.78	-1.13	0.00	0.00	3.91	0.00	0.08
010–O2-Mg1	+0.34	-0.34	+1.21	+0.79	-1.13	0.00	0.00	3.92	0.00	0.08
010–O1-O1	+0.29	+0.29	-0.13	+1.14	-1.05	-0.03	-0.03	4.06	0.00	0.00
010–O1-O2	+0.29	+0.31	+0.54	+0.47	-1.05	0.03	-0.03	4.88	-0.92	0.04
010–O2-O2	+0.30	+0.30	+1.22	-0.16	-1.05	0.00	0.00	3.92	0.00	0.08

Table S7. Adsorption energies (in kJ mol^{-1}) calculated at the BHLYP/B2//BHLYP/B1 level for the global H adsorption processes on Ol(010) to form the 010–Fe1-Mg1, 010–Fe1-O1, 010–Fe1-O2, 010–O1-Mg1, 010–O2-Mg1, 010–O1-O1, 010–O1-O2 and 010–O2-O2 complexes at quintet and heptet spin state.

Reaction	Spin	ΔE_{el}
Ol(010) + 2H → 010–Fe1-Mg1	Quintet	-172.4
	Heptet	-171.3
Ol(010) + 2H → 010–Fe1-O1	Quintet	-421.5
	Heptet	-129.8
Ol(010) + 2H → 010–Fe1-O2	Quintet	-214.4
	Heptet	-214.2
Ol(010) + 2H → 010–O1-Mg1	Quintet	-325.5
	Heptet	-54.6
Ol(010) + 2H → 010–O2-Mg1	Quintet	-398.8
	Heptet	-129.8
Ol(010) + 2H → 010–O1-O1	Quintet	-160.3
	Heptet	-130.1
Ol(010) + 2H → 010–O1-O2	Quintet	-80.8
	Heptet	-75.8
Ol(010) + 2H → 010–O2-O2	Quintet	-108.6
	Heptet	-107.9

Table S8. Reaction energies (in kJ mol^{-1}) calculated at the B3LYP-D2*/B2//B3LYP-D2*/B1 and BHLYP-D2*/B2//BHLYP/B1 level, respectively, for the H_2 formation processes on Ol(010) from the most significant doubly-H adsorption complexes at quintet spin state.

Method	Adduct	ΔE_{el}	ΔE_{D2^*}	ΔE	ΔZPE	ΔU_0
010–Fe1-Mg1 → 010–Fe-H_2						
B3LYP-D2*	010–Fe1-Mg1	-192.8	-5.1	-197.9	20.2	-177.7
	TS1-H_2	-186.3	-6.6	-192.9	18.8	-174.1
	010–Fe1-H_2	-475.2	-7.5	-482.7	39.8	-442.9
BHLYP-D2*	010–Fe1-Mg1	-172.4	-5.1	-177.5	21.1	-156.4
	TS1-H_2	-165.8	-6.6	-172.4	19.4	-153.0
	010–Fe1-H_2	-465.9	-7.5	-473.4	40.1	-433.3
010–O2-Mg1 → 010–Mg-H_2						
B3LYP-D2*	010–O2-Mg1	-408.6	-4.8	-413.4	41.3	-372.1
	TS2-H_2	-391.6	-9.1	-400.7	30.9	-369.8
	010–Mg1-H_2	-471.8	-9.2	-481.0	36.0	-445.0
BHLYP-D2*	010–O2-Mg1	-398.8	-4.8	-403.6	43.0	-360.6
	TS2-H_2	-364.8	-9.1	-373.9	31.6	-342.3
	010–Mg1-H_2	-467.5	-9.2	-476.7	36.1	-440.6
010–Fe1-O1 → 010–Fe-H_2						
B3LYP-D2*	010–Fe1-O1	-419.3	-4.7	-424.0	43.0	-381.0
	TS3-H_2	-375.7	-10.0	-385.7	31.2	-354.5
	010–Fe1-H_2	-475.2	-7.5	-482.7	39.8	-442.9
BHLYP-D2*	010–Fe1-O1	-421.5	-4.7	-426.2	44.8	-381.4
	TS3-H_2	-365.9	-10.0	-375.9	32.3	-343.6
	010–Fe1-H_2	-465.9	-7.5	-473.4	40.1	-433.3

Table S9. Adsorption energies (in kJ mol^{-1}) calculated at the B3LYP-D2*/B2//B3LYP-D2*/B1 and BHLYP-D2*/B2//BHLYP/B1 level, respectively, for the H_2 molecule on Ol(010).

Reaction	Method	ΔE_{el}	ΔE_{D2^*}	ΔE	ΔZPE	ΔU_0
Ol(010) + H_2 → 010–Mg1-H_2	B3LYP-D2*	-11.4	-9.2	-20.6	9.4	-11.2
	BHLYP-D2*	-14.3	-9.2	-23.5	8.8	-14.7
Ol(010) + H_2 → 010–Fe1-H_2	B3LYP-D2*	-14.8	-7.5	-22.3	13.3	-9.0
	BHLYP-D2*	-12.7	-7.5	-20.2	12.9	-7.3

Table S10. B3LYP-D2*/B2//B3LYP-D2*/B1 and BHLYP-D2*/B2//BHLYP/B1 zero-point energy corrected energy barriers ($\Delta U_0^{\ddagger}$, in kJ mol^{-1}), transition frequencies ($\nu^{\ddagger}$, in cm^{-1}) and tunnelling crossover temperatures (T_X, in K) on Ol(010).

Reaction	Method	$\Delta U_0^{\ddagger}$	$\nu^{\ddagger}$	T_X
010–Fe1-Mg1 → 010–Fe-H_2	B3LYP-D2*	3.6	144	35
	BHLYP-D2*	3.4	82	19
010–O2-Mg1 → 010–Mg-H_2	B3LYP-D2*	2.3	1077	610
	BHLYP-D2*	18.3	1405	358
010–Fe1-O1 → 010–Fe-H_2	B3LYP-D2*	26.5	1287	315
	BHLYP-D2*	37.8	1445	349

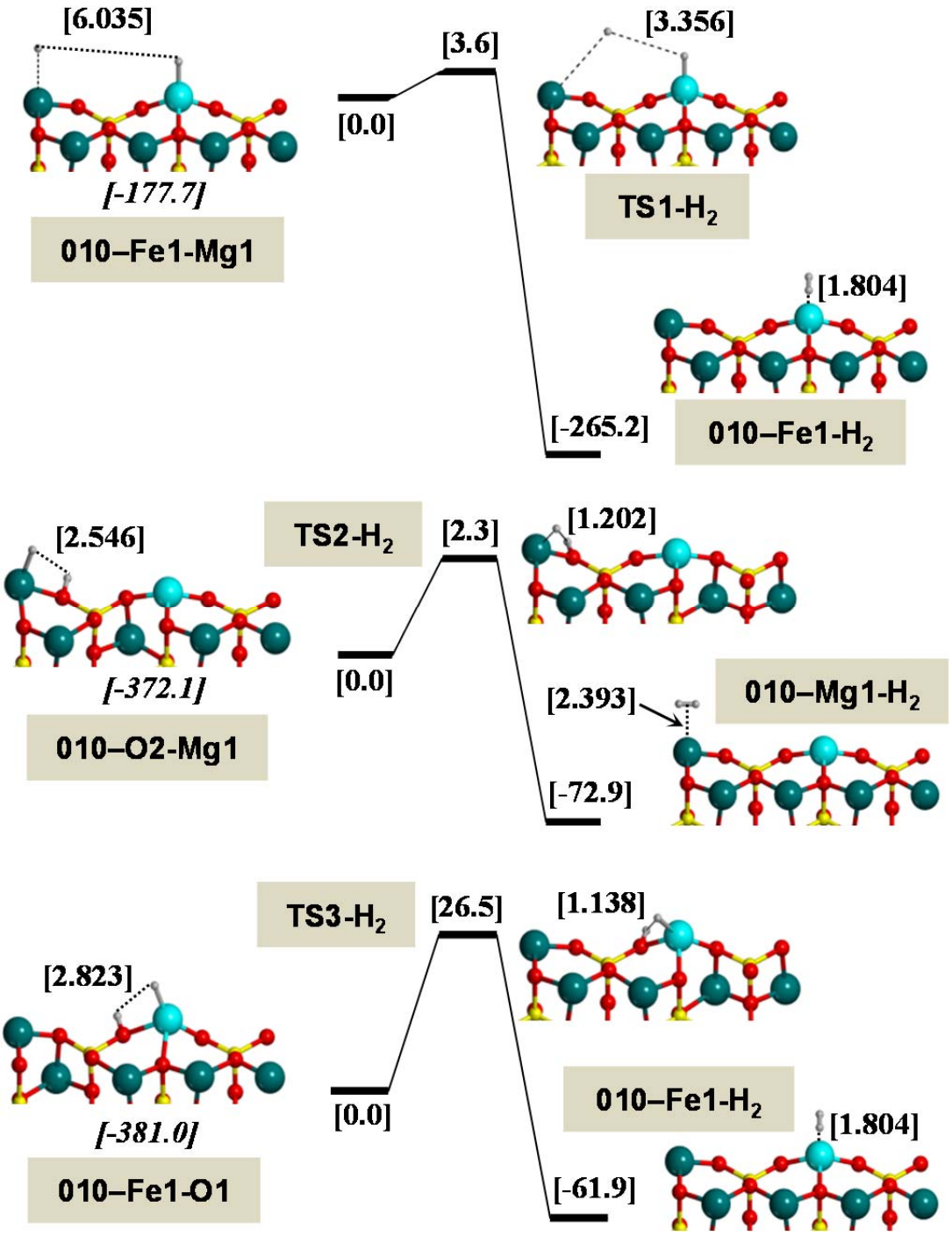

Figure S5. B3LYP-D2*-energy profiles including zero-point energy corrections (in kJ mol^{-1}) for H_2 formation from the most significant doubly-H adsorption complexes. All the structures are calculated in the quintet state, which are more stable than the heptet state (see Table S7). Adsorption energies (values in italics above the reactants) are referenced with respect to the Ol(010) + 2H zero-energy asymptote, whereas values of the energy profiles are referenced with respect to the corresponding reactants. Bond distances in Å.

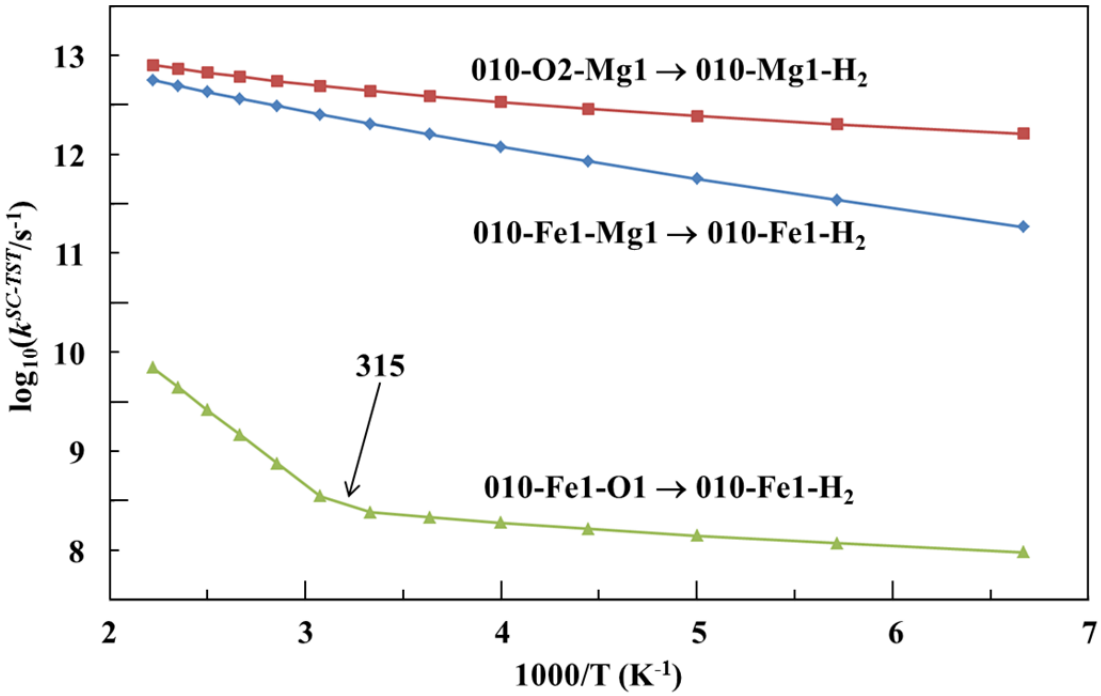

Figure S6. Arrhenius plots of k^{SC-TST} between 150 and 450 K for the H_2 formation processes at B3LYP-D2*/B2//B3LYP-D2*/B1 level. Crossover temperatures (T_X, in K) are also indicated.